On the Achievable Rate of IRS-Assisted Multigroup Multicast Systems

Muhammad Farooq*, Vaibhav Kumar*, Markku Juntti†, and Le-Nam Tran*
*School of Electrical and Electronic Engineering, University College Dublin, Belfield, Dublin 4, Ireland
†Centre for Wireless Communications, University of Oulu, P.O. Box 4500, FI-90014, Finland
Email: muhammad.farooq@ucdconnect.ie; vaibhav.kumar@ieee.org; markku.juntti@oulu.fi; nam.tran@ucd.ie

***Abstract*—Intelligent reflecting surfaces (IRSs) have shown huge advantages in many potential use cases and thus have been considered a promising candidate for next-generation wireless systems. In this paper, we consider an IRS-assisted multigroup multicast (IRS-MGMC) system in a multiple-input single-output (MISO) scenario, for which the related existing literature is rather limited. In particular, we aim to jointly design the transmit beamformers and IRS phase shifts to maximize the sum rate of the system under consideration. In order to obtain a numerically efficient solution to the formulated non-convex optimization problem, we propose an *alternating projected gradient* (APG) method where each iteration admits a closed-form and is shown to be superior to a known solution that is derived from the majorization-minimization (MM) method in terms of both achievable sum rate and required complexity, i.e., run time. In particular, we show that the complexity of the proposed APG method grows *linearly* with the number of IRS tiles, while that of the known solution in comparison grows with the third power of the number of IRS tiles. The numerical results reported in this paper extend our understanding on the achievable rates of large-scale IRS-assisted multigroup multicast systems.**

***Index Terms*—Intelligent reflecting surface, multigroup multicast, alternating projected gradient, multiple-input single-output.**

I. Introduction

With the advent of new wireless communication services and an unprecedented increase in the number of wireless devices, the problem of supporting massive connectivity in the very-congested sub-6 GHz spectrum band has become a challenging problem for beyond fifth generation (B5G)/sixth generation (6G) wireless standards. In this context, services like audio/video streaming are supported via the evolved multimedia broadcast/multicast service (eMBMS) in the third-generation partnership project (3GPP) [1], [2]. In such a media streaming scenario, multiple users in a group are served with the same content, whereas the content delivered among the groups is mutually independent. This indeed has motivated several pioneer works on physical layer multicasting [3], [4].

On the other hand, intelligent reflecting surfaces (IRSs) are being envisioned as a disruptive technology to enhance the performance of next-generation wireless [5]. These IRSs are capable of steering the incident radio waves in the desired direction to improve a certain performance measure. Therefore, optimal system design for IRS-assisted physical layer multicasting has naturally gained increasing interest in recent years. Some of the recent works on IRS-assisted *single-group* multicast system design include [6]–[8], whereas those on IRS-assisted *multigroup* multicast (IRS-MGMC) system design include [9]–[11].

In particular, Zou *et al.* in [9] considered the problem of sum rate maximization in a multiple-input single-output (MISO) IRS-MGMC system, where they aim to jointly design the optimal transmit beamforming vectors and IRS phase shifts via alternating optimization (AO). More specifically, they proposed two different optimization schemes based on majorization-minimization (MM). The first one involved second-order cone programming (SOCP) which requires high complexity, while the second scheme was based on a smoothing technique and admitted closed-form expressions, and thus had lower complexity. We refer to the latter as the MM method for short in the rest of the paper. The problem of transmit power minimization in an MISO IRS-MGMC system subject to some quality-of-service (QoS) constraints was presented in [10], where the optimal transmit beamformers and IRS phase shifts were obtained using a difference-of-convex (DC) algorithm in conjunction with the AO. Similarly, in [11], the problem of transmit power minimization subject to multiple QoS constraints in an IRS-MGMC symbiotic radio was considered, where optimal transmit and reflect structures were obtained using AO, quadratic transform, and semidefinite programming (SDP).

It is worth mentioning that in a practical system, the number of passive reflecting tiles in the IRS will be in the order of a few hundred, if not thousands [12]. This massive number of reflecting elements will likely contribute the most toward the total complexity of any optimal system design. Therefore, for the IRS-MGMC sum rate maximization problem, the MM method in [9, Algorithm 2], whose complexity has a cubic growth with the number of IRS tiles, is still impractical for large systems. Also, as shall be seen later, the MM method in [9] does not perform well in the high power regime since the derived bounds were not tight in this case. Due to the shortcomings of the previous studies, in this paper, we propose a first-order method based on *alternating projected gradient* (APG), which results in superior performance and lower complexity compared to that of the MM method in [9]. Our main contributions in this paper are as follows:

(i) We propose a low-complexity APG algorithm to obtain optimal transmit and reflect structures for sum rate

This publication has emanated from research conducted with the financial support of Science Foundation Ireland (SFI) and is co-funded under the European Regional Development Fund under Grant Number 17/CDA/4786.

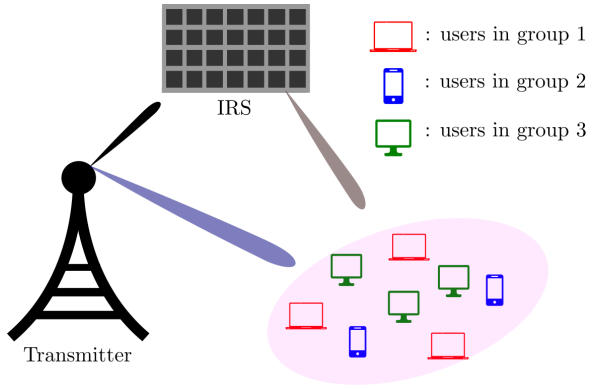

Fig. 1. An example IRS-assisted multigroup multicast system model with $K = 8$, $G = 3$, $K_1 = K_3 = 3$, and $K_2 = 2$.

maximization in an MISO IRS-MGMC system, which is shown to outperform the benchmark MM method, i.e. [9, Algorithm 2].

(ii) We provide a detailed complexity analysis of the proposed APG algorithm which confirms that the per-iteration complexity of our proposed algorithm *grows linearly* with the number of IRS tiles, which is significantly less than that of the benchmark MM method. In particular, our implementation indicates that the proposed APG method is $1000\times$ faster when the number of reflecting elements is 400.

(iii) Extensive numerical results are provided to evaluate the performance of our proposed algorithm, and to analyze the effect of different system parameters of interest on the system performance, showing that the IRS can improve significantly the achievable sum rate in multigroup multicasting scenarios. Specifically, the gain of the proposed solution is up to 50% compared to the MM method.

Notations: Bold uppercase and lowercase letters are used to denote matrices and vectors, respectively. The Hermitian, transpose and Euclidean norm of a vector $\mathbf{x}$ are, respectively, denoted by $\mathbf{x}^{\dagger}$, $\mathbf{x}^{\mathrm{T}}$ and $\|\mathbf{x}\|$. The absolute value of a complex number x is denoted by $|x|$. The vector space of all $M \times N$ complex-valued matrices is denoted by $\mathbb{C}^{M\times N}$. By $\mathrm{diag}(\mathbf{x})$, we represent a square diagonal matrix whose main diagonal consists of the elements of vector $\mathbf{x}$, whereas, $\mathrm{vec_d}(\mathbf{X})$ represents the column vector whose elements are the same as that of the main diagonal of the matrix $\mathbf{X}$. The operation $\ln(\cdot)$ represents the natural logarithm of the argument. The trace of the matrix $\mathbf{X}$ is denoted by $\mathrm{Tr}(\mathbf{X})$. Euclidean projection of a given vector $\mathbf{x}$ onto the set $\mathcal{X}$ is defined as $\Pi_{\mathcal{X}}(\mathbf{x}) \triangleq \min_{\hat{\mathbf{x}}\in\mathcal{X}} \|\hat{\mathbf{x}} - \mathbf{x}\|$. The expected value of a random variable is denoted by $\mathbb{E}\{\cdot\}$. By $\mathcal{O}(\cdot)$, we denote the Landau symbol. Finally, we denote by $\nabla_{\mathbf{x}} f(\cdot)$ the complex gradient of $f(\cdot)$ with respect to $\mathbf{x}^*$, i.e., $\nabla_{\mathbf{x}} f(\cdot) \equiv \frac{\partial}{\partial \mathbf{x}^*} f(\cdot) = \frac{1}{2}\left(\frac{\partial f(\cdot)}{\partial \Re(\mathbf{x})} + j\frac{\partial f(\cdot)}{\partial \Im(\mathbf{x})}\right)$ [13, Chap. 3].

II. System Model and Problem Formulation

Consider an IRS-assisted multigroup multicast system shown in Fig. 1, consisting of one transmitter, one (passive) IRS, and K users. We assume that the transmitter is equipped with N antennas, the IRS consists of M low-cost passive reflecting tiles, and all of the users are single-antenna nodes. The users are divided into G groups, where the set of groups is denoted by $\mathcal{G} \triangleq \{1, 2, \ldots, G\}$. We denote by $\mathrm{U}_{k,g}$ the k-th user in the g-th group. The set of users in each group $g \in \mathcal{G}$ is denoted by $\mathcal{U}_g \triangleq \{\mathrm{U}_{k,g} \mid k \in \mathcal{K}_g\}$ where $\mathcal{K}_g \triangleq \{1, 2, \ldots, K_g\}$ and K_g denotes the number of users in the g-th group. We assume that all of the users in one group receive the same message from the transmitter, while the message intended for each group is independent from those for the other groups. In this paper we adopt a beamforming approach for each group. Thus, the signal at the transmitter is therefore given by

$$\mathbf{x} = \sum\nolimits_{g\in\mathcal{G}} \mathbf{f}_g v_g, \tag{1}$$

where $\mathbf{f}_g \in \mathbb{C}^{N\times 1}$ is the beamforming vector for the g-th group and v_g is the information-bearing Gaussian symbol intended for the g-th group such that $\mathbb{E}\{|v_g|^2\} = 1$. We define $\mathbf{f} \triangleq [\mathbf{f}_1^{\mathrm{T}}, \mathbf{f}_2^{\mathrm{T}}, \ldots, \mathbf{f}_G^{\mathrm{T}}]^{\mathrm{T}} \in \mathbb{C}^{NG\times 1}$ to be the vector stacking the beamforming vectors of all of the groups. We assume that the instantaneous channel state information (CSI) is perfectly known at all of the nodes[1]. Let the transmitter-IRS, transmitter-$\mathrm{U}_{k,g}$, and IRS-$\mathrm{U}_{k,g}$ links are denoted by $\mathbf{H}_{\mathrm{ts}} \in \mathbb{C}^{M\times N}$, $\mathbf{h}_{k,g} \in \mathbb{C}^{1\times N}$, and $\hat{\mathbf{h}}_{k,g} \in \mathbb{C}^{1\times M}$, respectively. Then, the received signal at $\mathrm{U}_{k,g}$ is expressed as

$$y_{k,g} = \left(\mathbf{h}_{k,g} + \hat{\mathbf{h}}_{k,g}\boldsymbol{\Theta}\mathbf{H}_{\mathrm{ts}}\right)\mathbf{x} + w_{k,g}, \tag{2}$$

where $w_{k,g} \sim \mathcal{CN}(0, \sigma^2)$ is the additive white Gaussian noise at $\mathrm{U}_{k,g}$, $\boldsymbol{\Theta} \triangleq \mathrm{diag}(\boldsymbol{\theta})$ with $\boldsymbol{\theta} \triangleq [\theta_1, \theta_2, \ldots, \theta_M]^{\mathrm{T}} \in \mathbb{C}^{M\times 1}$ denoting the IRS phase shift vector, $\theta_m \triangleq \exp(j\phi_m)$, $\forall m \in \mathcal{M} \triangleq \{1, 2, \ldots, M\}$, and $\phi_m \in [0, 2\pi)$. With a slight abuse of notation, in the sequel of the paper, we normalize the involving channels appropriately with the noise power, i..e, $\mathbf{h}_{k,g} \leftarrow \mathbf{h}_{k,g}/\sigma$ and $\hat{\mathbf{h}}_{k,g} \leftarrow \hat{\mathbf{h}}_{k,g}/\sigma$, and thus the resulting equivalent noise has a unit variance. In addition to lightening the notations, this normalization step also has a numerical benefit in the sense that we do not need to deal directly with extremely small quantities such as the channels and the noise power themselves. In this way, the achievable rate (in nats/s/Hz) at $\mathrm{U}_{k,g}$ is given by[2]

$$R_{g,k}(\mathbf{f}, \boldsymbol{\theta}) = \ln\left(1 + \frac{|\mathbf{z}_{g,k}\mathbf{f}_g|^2}{1 + \sum_{\ell\in\mathcal{G}\setminus\{g\}} |\mathbf{z}_{k,g}\mathbf{f}_\ell|^2}\right), \tag{3}$$

where $\mathbf{z}_{k,g} \triangleq \mathbf{h}_{k,g} + \hat{\mathbf{h}}_{k,g}\boldsymbol{\Theta}\mathbf{H}_{\mathrm{ts}}$. We emphasize that $\mathbf{z}_{k,g}$ depends on the phase shifts, although the notation does not explicitly show this. Since all of the users in the g-th group needs to correctly decode the intended message, i.e., v_g, the achievable rate for the g-th group is defined as

$$\mathcal{R}_g(\mathbf{f}, \boldsymbol{\theta}) = \min\nolimits_{k\in\mathcal{K}_g}\{R_{k,g}(\mathbf{f}, \boldsymbol{\theta})\}. \tag{4}$$

In this paper, we aim to jointly design the optimal transmit beamformers $(\mathbf{f}_g, \forall g \in \mathcal{G})$ and IRS phase shifts $(\theta_m, \forall m \in \mathcal{M})$ to maximize achievable sum rate of all of the groups. The

[1]A similar assumption on the perfect CSI availability was considered in [6], [9]–[11], [14]. Also, since in this paper our main motivation is to provide an efficient low-complexity algorithm for the sum rate maximization problem in an IRS-MGMC system, the problem of channel estimation is out of scope of this paper.

[2]For mathematical convenience, we express the achievable rate in nats/s/Hz. However, the results in Section IV are shown for achievable rate in bps/Hz, which is more commonly used.

optimization problem can therefore be mathematically stated as

$$\underset{\mathbf{f},\boldsymbol{\theta}}{\text{maximize}} \ \left\{\mathcal{R}_{\text{sum}}(\mathbf{f},\boldsymbol{\theta}) \triangleq \sum\nolimits_{g\in\mathcal{G}} \mathcal{R}_g(\mathbf{f},\boldsymbol{\theta})\right\} \tag{5a}$$

$$\text{subject to } \|\mathbf{f}\| \leq \sqrt{P_{\text{t}}}, \tag{5b}$$

$$|\theta_m| = 1, \forall m \in \mathcal{M}, \tag{5c}$$

where P_{t} is the maximum transmit power available at the transmitter. The constraint in (5b) denotes the transmit power constraint at the transmitter, and those in (5c) represent the unit-modulus constraints at the reflecting tiles[3]. Note that the problem in (5) is non-convex due to the coupling between the optimization variables $\mathbf{f}$ and $\boldsymbol{\theta}$ in (5a), and the non-convex constraints in (5c). It is also noteworthy that (5a) is non-differentiable due to the inherent piecewise minimization operator in (4). These two challenges make it difficult to develop efficient methods for solving (5).

Before describing our proposed solution in the next section, we provide an important remark regarding an existing solution to (5), proposed in [9, Algorithm 1] based on the MM method. In particular, the authors first obtained a *concave lower bound* on (5a) when $\mathbf{f}$ or $\boldsymbol{\theta}$ are fixed and then maximize the derived lower bound. This process is repeated alternatively between $\mathbf{f}$ and $\boldsymbol{\theta}$ until convergence. In particular, it was shown that the resulting per-iteration complexity of this method is $\mathcal{O}(M^{3.5})$ [4]. Furthermore, in order to reduce the complexity, the authors in [9, Algorithm 2] also proposed the MM method with the per-iteration complexity of $\mathcal{O}(K(M+1)^3)$ based on a smoothing technique. From the complexity perspective, it is obvious that both methods are still not practically appealing for large M which is expected to be the case for the IRS to have a significant impact. Thus, developing a more efficient algorithm for solving (5) is still of huge interest.

III. Proposed Solution

In this section, we propose a low-complexity algorithm to find a stationary solution to the problem in (5), and show that the complexity of our proposed algorithm grows *linearly* with the number of tiles at the IRS.

A. The Alternating Projected Gradient (APG) Algorithm

First, to tackle the nonsmoothness of the objective, we apply a smoothing technique introduced in [16]. We remark that although a smoothing techniques is also used in [9], the difference is that in this paper, we apply the smoothing on the true objective, i.e., on (5a), whereas in [9], the same smoothing was applied to a concave lower-bound on (5a). As shall be demonstrated in the next section, it turns out that this difference creates a huge impact on the achievable rate. Specifically, a differentiable approximation of (5a) is found as [16]

$$\begin{aligned}\mathcal{R}_{\text{sum}}(\mathbf{f},\boldsymbol{\theta}) &\approx -\frac{1}{\tau}\sum\nolimits_{g\in\mathcal{G}} \ln\Big[\sum\nolimits_{k\in\mathcal{K}_g} \exp\left\{-\tau R_{k,g}(\mathbf{f},\boldsymbol{\theta})\right\}\Big] \\ &\triangleq \tilde{\mathcal{R}}_{\text{sum}}(\mathbf{f},\boldsymbol{\theta}),\end{aligned} \tag{6}$$

[3]Many different IRS phase shift models are suggested in literature [12], [15], however, the unit-modulus model is the most frequently used one [5]–[11], [14].

[4]In a practical IRS-MGMC system, $M \gg \max\{N,K,G\}$, and therefore we neglect the lower-order terms.

Algorithm 1: The proposed alternating projected gradient (APG) algorithm for solving (7)

Input: $\mathbf{f}^{(0)}$, $\boldsymbol{\theta}^{(0)}$, $\alpha_{\mathbf{f}}$, $\alpha_{\boldsymbol{\theta}}$, $\tau > 0$
Output: $\mathbf{f}^{\star}$, $\boldsymbol{\theta}^{\star}$

$n \leftarrow 1$
repeat
  $\mathbf{f}^{(n)} = \Pi_{\mathcal{F}}\big(\mathbf{f}^{(n-1)} + \alpha_{\mathbf{f}} \nabla_{\mathbf{f}} \tilde{\mathcal{R}}_{\text{sum}}\big(\mathbf{f}^{(n-1)}, \boldsymbol{\theta}^{(n-1)}\big)\big)$;
  $\boldsymbol{\theta}^{(n)} = \Pi_{\Theta}\big(\boldsymbol{\theta}^{(n-1)} + \alpha_{\boldsymbol{\theta}} \nabla_{\boldsymbol{\theta}} \tilde{\mathcal{R}}_{\text{sum}}\big(\mathbf{f}^{(n)}, \boldsymbol{\theta}^{(n-1)}\big)\big)$;
  $n \leftarrow n+1$;
until *convergence*;
$\mathbf{f}^{\star} \leftarrow \mathbf{f}^{(n)}$, $\boldsymbol{\theta}^{\star} \leftarrow \boldsymbol{\theta}^{(n)}$

where $\tau > 0$ is the smoothing parameter, which also determines the accuracy of the approximation. Therefore, the problem in (5) is modified to the following problem

$$\underset{\mathbf{f},\boldsymbol{\theta}}{\text{maximize}} \ \tilde{\mathcal{R}}_{\text{sum}}(\mathbf{f},\boldsymbol{\theta}), \tag{7a}$$

$$\text{subject to (5b), (5c).}$$

For ease of exposition, we define the feasible set for $\mathbf{f}$ and $\boldsymbol{\theta}$ by $\mathcal{F} \triangleq \{\mathbf{f} \in \mathbb{C}^{NG\times 1} |\ \|\mathbf{f}\| \leq \sqrt{P_{\text{t}}}\}$ and $\Theta = \{\boldsymbol{\theta} \in \mathbb{C}^{M\times 1} |\ |\theta_m| = 1, m \in \mathcal{M}\}$, respectively. We remark that the sets $\mathcal{F}$ and Θ are simple in the sense that their projection can be computed exactly by closed-form. This fact indeed motivates us to adopt the alternating projected gradient to solve (5). In this context, we first provide the (complex-valued) gradient of $\tilde{\mathcal{R}}_{\text{sum}}(\mathbf{f},\boldsymbol{\theta})$ with respect to (w.r.t.) $\mathbf{f}$. By definition, we can immediately write $\nabla_{\mathbf{f}} \tilde{\mathcal{R}}_{\text{sum}}(\mathbf{f},\boldsymbol{\theta})$ as

$$\begin{aligned}\nabla_{\mathbf{f}} \tilde{\mathcal{R}}_{\text{sum}}(\mathbf{f},\boldsymbol{\theta}) = \big[&\big(\nabla_{\mathbf{f}_1} \tilde{\mathcal{R}}_{\text{sum}}(\mathbf{f},\boldsymbol{\theta})\big)^{\text{T}}, \\ &\big(\nabla_{\mathbf{f}_2} \tilde{\mathcal{R}}_{\text{sum}}(\mathbf{f},\boldsymbol{\theta})\big)^{\text{T}}, \ldots, \big(\nabla_{\mathbf{f}_G} \tilde{\mathcal{R}}_{\text{sum}}(\mathbf{f},\boldsymbol{\theta})\big)^{\text{T}}\big]^{\text{T}},\end{aligned} \tag{8}$$

where $\nabla_{\mathbf{f}_i} \tilde{\mathcal{R}}_{\text{sum}}(\mathbf{f},\boldsymbol{\theta}), i \in \mathcal{G}$, is provided by the following theorem.

Theorem 1. *A closed-form expression for* $\nabla_{\mathbf{f}_i} \tilde{\mathcal{R}}_{\text{sum}}(\mathbf{f},\boldsymbol{\theta})$ *is given by* (9)*, shown at the top of the next page, where* $\nabla_{\mathbf{f}_i} R_{k,i}(\mathbf{f},\boldsymbol{\theta}) = \frac{\mathbf{z}_{k,i}^{\dagger}\mathbf{z}_{k,i}\mathbf{f}_i}{1+\sum_{g\in\mathcal{G}}|\mathbf{z}_{k,i}\mathbf{f}_g|^2}$ *and* $\nabla_{\mathbf{f}_i} R_{k,\ell}(\mathbf{f},\boldsymbol{\theta}) = \big[\big(1 + \sum_{g\in\mathcal{G}}|\mathbf{z}_{k,\ell}\mathbf{f}_g|^2\big)^{-1} - \big(1+\sum_{j\in\mathcal{G}\setminus\{\ell\}}|\mathbf{z}_{k,\ell}\mathbf{f}_j|^2\big)^{-1}\big]\mathbf{z}_{k,\ell}^{\dagger}\mathbf{z}_{k,\ell}\mathbf{f}_i$.

Proof: See Appendix A. ∎

Next, we obtain a closed-form expression for the gradient of $\tilde{\mathcal{R}}_{\text{sum}}(\mathbf{f},\boldsymbol{\theta})$ w.r.t. $\boldsymbol{\theta}$ as given below.

Theorem 2. *A closed-form expression for* $\nabla_{\boldsymbol{\theta}} \tilde{\mathcal{R}}_{\text{sum}}(\mathbf{f},\boldsymbol{\theta})$ *is given by* (10)*, shown at the top of the next page, where* $\nabla_{\boldsymbol{\theta}}|\mathbf{z}_{k,g}\mathbf{f}_i|^2 = \text{vec}_{\text{d}}\left\{\big(\hat{\mathbf{h}}_{k,g}\big)^{\dagger}\mathbf{z}_{k,g}\mathbf{f}_i\mathbf{f}_i^{\dagger}\mathbf{H}_{\text{ts}}^{\dagger}\right\}$.

Proof: See Appendix B. ∎

Equipped with **Theorems 1** and **2**, we are now in a position to described the proposed APG algorithm to obtain a stationary solution to (7). The APG algorithm is summarized in **Algorithm 1**, where $\mathbf{f}^{(n)}$ and $\boldsymbol{\theta}^{(n)}$ denote the (stacked) transmit beamformers and IRS phase shifts in the n-th iteration, respectively, and $\alpha_{\mathbf{f}}$ and $\alpha_{\boldsymbol{\theta}}$ denote the step size corresponding to $\mathbf{f}$ and $\boldsymbol{\theta}$, respectively. Given the previous iteration $\mathbf{f}^{(n-1)}$, to increase the objective, we move along its gradient direction with a step size $\alpha_{\mathbf{f}}$ to obtain $\hat{\mathbf{f}}^{(n)} \triangleq \mathbf{f}^{(n-1)} + \alpha_{\mathbf{f}} \nabla_{\mathbf{f}} \tilde{\mathcal{R}}_{\text{sum}}\big(\mathbf{f}^{(n-1)}, \boldsymbol{\theta}^{(n-1)}\big)\big)$ and then project $\hat{\mathbf{f}}^{(n)}$ onto

$$\nabla_{\mathbf{f}_i}\tilde{\mathcal{R}}_{\rm sum}(\mathbf{f},\boldsymbol{\theta})=\frac{\sum_{k\in\mathcal{K}_i}\left[\exp\left\{-\tau R_{k,i}(\mathbf{f},\boldsymbol{\theta})\right\}\nabla_{\mathbf{f}_i}R_{k,i}(\mathbf{f},\boldsymbol{\theta})\right]}{\sum_{k\in\mathcal{K}_i}\exp\left\{-\tau R_{k,i}(\mathbf{f},\boldsymbol{\theta})\right\}}+\sum_{\ell\in\mathcal{G}\setminus\{i\}}\frac{\sum_{k\in\mathcal{K}_\ell}\left[\exp\left\{-\tau R_{k,\ell}(\mathbf{f},\boldsymbol{\theta})\right\}\nabla_{\mathbf{f}_i}R_{k,\ell}(\mathbf{f},\boldsymbol{\theta})\right]}{\sum_{k\in\mathcal{K}_\ell}\exp\left\{-\tau R_{k,\ell}(\mathbf{f},\boldsymbol{\theta})\right\}}. \tag{9}$$

$$\nabla_{\boldsymbol{\theta}}\tilde{\mathcal{R}}_{\rm sum}(\mathbf{f},\boldsymbol{\theta})=\sum\nolimits_{g\in\mathcal{G}}\frac{\sum_{k\in\mathcal{K}_g}\left[\exp\left\{-\tau R_{k,g}(\mathbf{f},\boldsymbol{\theta})\right\}\left\{\frac{\sum_{j\in\mathcal{G}}\nabla_{\boldsymbol{\theta}}|\mathbf{z}_{k,g}\mathbf{f}_j|^2}{1+\sum_{j\in\mathcal{G}}|\mathbf{z}_{k,g}\mathbf{f}_j|^2}-\frac{\sum_{\ell\in\mathcal{G}\setminus\{j\}}\nabla_{\boldsymbol{\theta}}|\mathbf{z}_{k,g}\mathbf{f}_\ell|^2}{1+\sum_{\ell\in\mathcal{G}\setminus\{j\}}|\mathbf{z}_{k,g}\mathbf{f}_\ell|^2}\right\}\right]}{\sum_{k\in\mathcal{K}_g}\exp\left\{-\tau R_{k,g}(\mathbf{f},\boldsymbol{\theta})\right\}}. \tag{10}$$

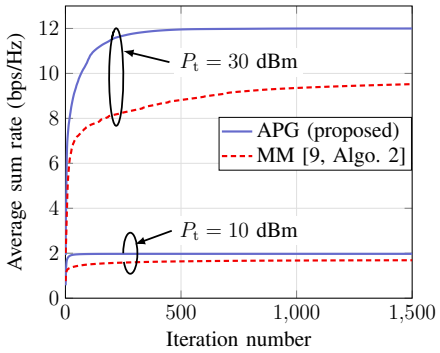

Fig. 2. Convergence of the APG and MM algorithms for $M=100$ and $G=K_g=3,\forall g\in\mathcal{G}$.

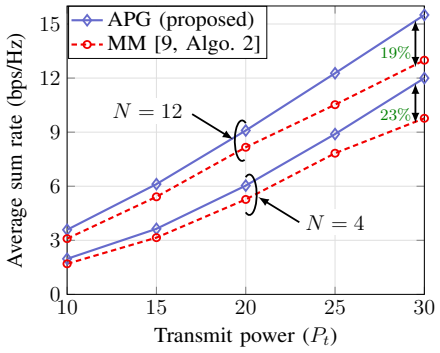

Fig. 3. Average sum rate versus the transmit power for $G=K_1=K_2=2$ and $M=100$.

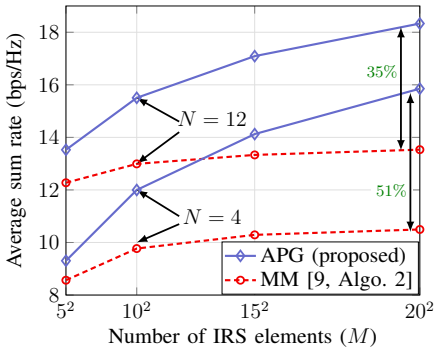

Fig. 4. Average sum rate versus M for $G=K_1=K_2=2$ and $P_{\rm t}=30$ dBm.

$\mathcal{F}$ to obtain $\mathbf{f}^{(n)}$, which is given by

$$\mathbf{f}^{(n)}=\Pi_{\mathcal{F}}\big(\hat{\mathbf{f}}^{(n)}\big)=\sqrt{P_{\rm t}}\hat{\mathbf{f}}^{(n)}\big/\max\left\{\|\hat{\mathbf{f}}^{(n)}\|,\sqrt{P_{\rm t}}\right\}. \tag{11}$$

In the same way, for a given $\hat{\boldsymbol{\theta}}^{(n)}=\big[\hat{\theta}_1^{(n)},\hat{\theta}_2^{(n)},\ldots,\hat{\theta}_M^{(n)}\big]^{\rm T}$, its projection onto Θ, i.e., $\Pi_{\Theta}\big(\hat{\boldsymbol{\theta}}^{(n)}\big)$, is given by $\boldsymbol{\theta}^{(n)}=\big[\theta_1^{(n)},\theta_2^{(n)},\ldots,\theta_M^{(n)}\big]^{\rm T}$, where

$$\theta_m^{(n)}=\begin{cases}\hat{\theta}_m^{(n)}/|\hat{\theta}_m^{(n)}|, & \text{if } |\hat{\theta}_m^{(n)}|\neq 0\\ \exp(j\phi),\phi\in[0,2\pi), & \text{otherwise}\end{cases},\forall m\in\mathcal{M}. \tag{12}$$

It is noteworthy that appropriate values of $\alpha_{\mathbf{f}}$ and $\alpha_{\boldsymbol{\theta}}$ can be obtained using a *backtracking line search* scheme, based on Armijo–Goldstein condition [17]. Also, the proof of convergence of **Algorithm 1** follows from [18].

B. Complexity Analysis

We now present a detailed complexity analysis of the proposed APG algorithm, where we count the required number of complex-valued multiplications in each iteration in **Algorithm 1.** In particular, we show that the proposed algorithm has a complexity that grows linearly with the number of reflecting elements, which is a notable reduction compared to the methods in [9]. For the sake of tractability, in this section, we assume an equal number of users in each group and define $\bar{K}\triangleq K_i=K/G,\forall i\in\mathcal{G}$ as the number of users per group. It is easy to note that the computational complexity of **Algorithm 1** is dominated by those associated with projected gradient steps 3 and 4 in **Algorithm 1**.

First, we analyze the complexity of $\nabla_{\mathbf{f}}\tilde{\mathcal{R}}_{\rm sum}(\mathbf{f},\boldsymbol{\theta};\tau)$, which is mostly due to the associated computational complexities for computing $\nabla_{\mathbf{f}_i}R_{k,i}(\mathbf{f},\boldsymbol{\theta})$ and $\nabla_{\mathbf{f}_i}R_{k,\ell}(\mathbf{f},\boldsymbol{\theta})$ (see (9)). The complexity of computing $\mathbf{z}_{k,i}$ is of the order of $\mathcal{O}(MN)$ and computing K such terms requires $\mathcal{O}(KMN)$ multiplications. The complexities associated with computing $\mathbf{z}_{k,i}\mathbf{f}_i$, $(\mathbf{z}_{k,i})^{\dagger}\mathbf{z}_{k,i}\mathbf{f}_i$ and $\sum_{g\in\mathcal{G}}|\mathbf{z}_{k,i}\mathbf{f}_g|$ are then given by $\mathcal{O}(N)$, $\mathcal{O}(N)$ and $\mathcal{O}(GN)$. Therefore, it is clear from (15) that the computational complexity of $\nabla_{\mathbf{f}_i}R_{k,i}(\mathbf{f},\boldsymbol{\theta})$ is $\mathcal{O}(GN)$. Analogously, the computational complexity associated with $\nabla_{\mathbf{f}_i}R_{k,\ell}(\mathbf{f},\boldsymbol{\theta})$ is given by $\mathcal{O}(GN)$. From (9), it is then straightforward to see that the complexity of computing $\nabla_{\mathbf{f}_i}\tilde{\mathcal{R}}_{\rm sum}(\mathbf{f},\boldsymbol{\theta})$ is $\mathcal{O}(\bar{K}GN+(G-1)\bar{K}GN)=\mathcal{O}(KGN)$, and that for computing $\nabla_{\mathbf{f}}\tilde{\mathcal{R}}_{\rm sum}(\mathbf{f},\boldsymbol{\theta};\tau)$ is $\mathcal{O}(G^2KN)$. Note that the complexity of obtaining appropriate value of $\alpha_{\mathbf{f}}$ and that of $\Pi_{\mathcal{F}}(\cdot)$ will be negligible, and therefore, the per-iteration complexity of step 3 in **Algorithm 1** is equal to $\mathcal{O}(KNM+G^2KN)$.

Next, in order to estimate the complexity associated with the computation of $\nabla_{\boldsymbol{\theta}}\tilde{\mathcal{R}}_{\rm sum}(\mathbf{f},\boldsymbol{\theta})$, one needs to count the number of complex-valued multiplications required to compute $\nabla_{\boldsymbol{\theta}}|\mathbf{z}_{k,g}\mathbf{f}_j|^2$ and $\nabla_{\boldsymbol{\theta}}|\mathbf{z}_{k,g}\mathbf{f}_\ell|^2$ (see (10)). As given in (19), $\nabla_{\boldsymbol{\theta}}|\mathbf{z}_{k,g}\mathbf{f}_j|^2=\mathrm{vec_d}\left\{\big(\hat{\mathbf{h}}_{k,g}\big)^{\dagger}\mathbf{z}_{k,g}\mathbf{f}_j\mathbf{f}_j^{\dagger}\mathbf{H}_{\rm ts}^{\dagger}\right\}$, and since we have already computed $\mathbf{z}_{k,g}\mathbf{f}_j$ (see discussions in the preceding paragraph), the complexity of computing $\mathbf{z}_{k,g}\mathbf{f}_j\mathbf{f}_j^{\dagger}\mathbf{H}_{\rm ts}^{\dagger}$ is given by $\mathcal{O}(MN+M)$. Now since we only need to compute the diagonal elements of $\big(\hat{\mathbf{h}}_{k,g}\big)^{\dagger}\mathbf{z}_{k,g}\mathbf{f}_j\mathbf{f}_j^{\dagger}\mathbf{H}_{\rm ts}^{\dagger}$, the complexity associated with $\nabla_{\boldsymbol{\theta}}|\mathbf{z}_{k,g}\mathbf{f}_j|^2$ is given by $\mathcal{O}(MN+2M)$. Similarly, the computational complexity of $\nabla_{\boldsymbol{\theta}}|\mathbf{z}_{k,g}\mathbf{f}_\ell|^2$ is given by $\mathcal{O}(MN+2M)$. Therefore, the complexity associated with $\nabla_{\boldsymbol{\theta}}\tilde{\mathcal{R}}(\mathbf{f},\boldsymbol{\theta})$ is $\mathcal{O}(G^2\bar{K}(MN+2M)+G(G-1)\bar{K}(MN+2M))\approx\mathcal{O}(MKGN)$. The complexity of backtracking line search to obtain appropriate value of $\alpha_{\boldsymbol{\theta}}$ and that for $\Pi_{\Theta}(\cdot)$ is comparatively very small, and can therefore be neglected. Hence, the total complexity associated with step 4 in **Algorithm 1** will be the same as that of the $\nabla_{\boldsymbol{\theta}}\tilde{\mathcal{R}}(\mathbf{f},\boldsymbol{\theta})$.

From the discussions presented above, we can write the overall per-iteration complexity of **Algorithm 1** as

$$\mathcal{O}(MKGN+G^2KN). \tag{13}$$

Since in a practical IRS-MGMC system, the number of IRS

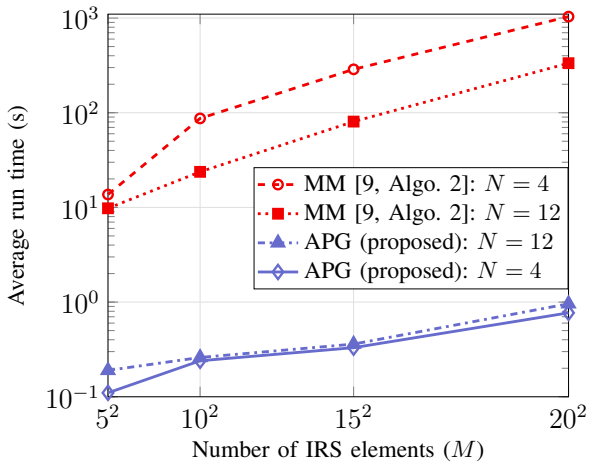

Fig. 5. Average run-time comparison between the proposed APG and the MM algorithms for $G = K_1 = K_2 = 2$ and $P_{\rm t} = 30$ dBm.

tiles is likely much larger than the number of transmit antennas, total number of users, or the total number of groups, i.e., $M \gg \max\{N, K, G\}$, the overall per-iteration complexity of **Algorithm 1** can be approximated by $\mathcal{O}(MKGN)$, which is linear w.r.t. the number of IRS tiles. Recall that as discussed in Sec. II, the complexity of the MM algorithm [9] has a cubic growth w.r.t. the number of tiles at the IRS.

IV. Numerical Results

In this section, we present the results of numerical experiments to evaluate the performance of the system under consideration. It is assumed that the uniform linear array at the transmitter is centered at (0 m, 20 m, 10 m), whereas the uniform planar array at the IRS is centered at (30 m, 0 m, 5 m). On the other hand, the users are assumed to be uniformly distributed in a circular area of radius 20 m, centered at (350 m, 50 m, 2 m). The center frequency of the carrier wave is set to 2 GHz. The distance between the adjacent antennas at the transmitter, and that between the adjacent tiles at the IRS is considered to be $\lambda/2$, with λ $(= 0.15$ m$)$ being the carrier wavelength. On the other hand, the minimum distance between the users is assumed to be equal to 2λ. The distance-dependent path loss and the Rician-distributed small-scale fading between the nodes are modeled following the arguments in [14, Sec. VI]. The noise power spectral density is equal to -174 dBm/Hz, and the total available bandwidth is 10 MHz. In Figs. 2–5, the average achievable sum rate/average run time is shown for 100 channel realizations. Also, we consider $\tau = 50$, and the tolerance for convergence is set to 10^{-5}.

In Fig. 2, we compare the convergence of the proposed APG algorithm with that of the baseline MM algorithm. It can be observed from the figure that the proposed APG algorithm outperforms the baseline MM algorithm, and the difference between the performance of the two algorithms increases with increasing transmit power. This is due to the reason that the tightness of the bounds used in [9, Algo. 2] for the MM algorithm depends on the transmit power and the involved channels. In particular, if the transmit power is small, then the bounds are relatively tight but are not so for a high transmit power (cf. [9, Appendix D]). The consequence is that the progress made in each iteration of the MM method is very small. Thus, even after a very large number of iterations, the MM algorithm still does not reaches a full convergence. It can also be observed that the proposed APG method requires quite many iterations to converge for high transmit power since in this case, the Lipschitz constant of the gradient of the objective is large, which forces the step size in each iteration to be small. However, since the per-iteration complexity is very small, the overall run-time for the APG algorithm is much lesser than that of the MM algorithm. We discuss the average run time for both the algorithms later in Fig. 5.

Next, in Fig. 3, we demonstrate the effect of transmit power on the achievable sum rate, and also the advantage of deploying more transmit antennas in the considered system. It can be observed from the figure that the proposed APG algorithm outperforms the MM algorithm for all considered scenarios. The performance difference between the two algorithms increases with increasing values of $P_{\rm t}$ due to the same reason as explained for Fig. 2. We also remark that the sum rate increases with an increase in the number of transmit antennas due to the multiplexing gains of MISO systems. The gains compared to the MM algorithms are clearly indicated in Fig 3.

In Fig. 4, we compare the sum rate performance of the proposed APG algorithm with that of the MM algorithm for an increasing number of IRS tiles. From the figure, it can be noticed that increasing the number of IRS tiles improves the achievable sum rate as a larger number of IRS tiles enables the IRS to perform highly-focused beamforming to maximize the achievable sum rate. Next, we observe that when the number of IRS tiles is increased, the rate of increase in the achievable sum rate is much higher in the case of the proposed APG method than the baseline MM method, where the gains compared to the MM algorithms are clearly marked in Fig 4.

In Fig. 5, we show the average rum time comparison between the proposed APG algorithm and the MM algorithm[5]. As described earlier, the complexity of the proposed APG algorithm grows linearly, in comparison to the cubic rate of increase in the complexity of the MM algorithm w.r.t. M. This result is in-line with that shown in Fig. 5, where for large value of M (say 400), the APG algorithm is 1000 times faster than the MM algorithm. The average run time of the APG algorithm increases when the number of transmit antennas increases, because the complexity of the proposed algorithm also grows with N (see (13)). Interestingly enough, for fixed values of M, K and G, the average run time of the MM algorithm decreases with increasing N. This occurs because, for a large value of N, the system has more degrees of freedom, which results in faster convergence of the algorithm (compared to the case when N is small). This in turn reduces the average run time for the MM algorithm when N is large.

[5]We are thankful to the authors of [9] for sending us the code for their proposed MM methods for comparison.

V. Conclusion

In this paper, we have considered the problem of sum rate maximization for an IRS-assisted multigroup multicast MISO system. In order to jointly design the optimal transmit beamformer and IRS phase shifts, we proposed a low-complexity alternating projected gradient method, that outperformed the benchmark schemes both in terms of performance and complexity. The complexity analysis confirmed that the complexity of the proposed algorithm increases linearly with the number of reflecting elements at the IRS, which is the best-known complexity result so far for such IRS-assisted systems. Extensive numerical results were provided to insight into the achievable rate performance of the IRS-MGMC system for different system parameters.

Appendix A
Proof of Theorem 1

Using (6), it is easy to note that

$$\begin{aligned}
&\nabla_{\mathbf{f}_i}\tilde{\mathcal{R}}_{\mathrm{sum}}(\mathbf{f},\boldsymbol{\theta})\\
&=\sum_{g\in\mathcal{G}}\frac{\sum_{k\in\mathcal{K}_g}\Big[\exp\big\{-\tau R_{k,g}(\mathbf{f},\boldsymbol{\theta})\big\}\nabla_{\mathbf{f}_i}R_{k,g}(\mathbf{f},\boldsymbol{\theta})\Big]}{\sum_{k\in\mathcal{K}_g}\exp\big\{-\tau R_{k,g}(\mathbf{f},\boldsymbol{\theta})\big\}}\\
&=\frac{\sum_{k\in\mathcal{K}_i}\Big[\exp\big\{-\tau R_{k,i}(\mathbf{f},\boldsymbol{\theta})\big\}\nabla_{\mathbf{f}_i}R_{k,i}(\mathbf{f},\boldsymbol{\theta})\Big]}{\sum_{k\in\mathcal{K}_i}\exp\big\{-\tau R_{k,i}(\mathbf{f},\boldsymbol{\theta})\big\}}\\
&+\sum_{\ell\in\mathcal{G}\setminus\{i\}}\frac{\sum_{k\in\mathcal{K}_\ell}\Big[\exp\big\{-\tau R_{k,\ell}(\mathbf{f},\boldsymbol{\theta})\big\}\nabla_{\mathbf{f}_i}R_{k,\ell}(\mathbf{f},\boldsymbol{\theta})\Big]}{\sum_{k\in\mathcal{K}_\ell}\exp\big\{-\tau R_{k,\ell}(\mathbf{f},\boldsymbol{\theta})\big\}}. \qquad (14)
\end{aligned}$$

Thus, to derive $\nabla_{\mathbf{f}_i}\tilde{\mathcal{R}}_{\mathrm{sum}}(\mathbf{f},\boldsymbol{\theta})$ we need to find $\nabla_{\mathbf{f}_i}R_{k,i}(\mathbf{f},\boldsymbol{\theta})$ and $\nabla_{\mathbf{f}_i}R_{k,\ell}(\mathbf{f},\boldsymbol{\theta})$ for $l\in\mathcal{G}\setminus\{i\}$. To this end using (3), we have

$$\begin{aligned}
\nabla_{\mathbf{f}_i}R_{k,i}(\mathbf{f},\boldsymbol{\theta})&=\nabla_{\mathbf{f}_i}\ln\Big(1+\sum_{g\in\mathcal{G}}|\mathbf{z}_{k,i}\mathbf{f}_g|^2\Big)\\
&\quad\underbrace{-\nabla_{\mathbf{f}_i}\ln\Big(1+\sum_{\ell\in\mathcal{G}\setminus\{i\}}|\mathbf{z}_{k,i}\mathbf{f}_\ell|^2\Big)}_{=\mathbf{0}}\\
&=\frac{\nabla_{\mathbf{f}_i}\big(\mathbf{z}_{k,i}\mathbf{f}_i\mathbf{f}_i^\dagger\mathbf{z}_{k,i}^\dagger\big)}{1+\sum_{g\in\mathcal{G}}|\mathbf{z}_{k,i}\mathbf{f}_g|^2}\overset{(a)}{=}\frac{\mathbf{z}_{k,i}^\dagger\mathbf{z}_{k,i}\mathbf{f}_i}{1+\sum_{g\in\mathcal{G}}|\mathbf{z}_{k,i}\mathbf{f}_g|^2}, \qquad (15)
\end{aligned}$$

where (a) follows from [13, Table 4.3]. Following similar steps, it can be shown that

$$\nabla_{\mathbf{f}_i}R_{k,\ell}(\mathbf{f},\boldsymbol{\theta})=\bigg(\frac{\mathbf{z}_{k,\ell}^\dagger\mathbf{z}_{k,\ell}\mathbf{f}_i}{1+\sum_{g\in\mathcal{G}}|\mathbf{z}_{k,\ell}\mathbf{f}_g|^2}-\frac{\mathbf{z}_{k,\ell}^\dagger\mathbf{z}_{k,\ell}\mathbf{f}_i}{1+\sum_{j\in\mathcal{G}\setminus\{\ell\}}|\mathbf{z}_{k,\ell}\mathbf{f}_j|^2}\bigg). \qquad (16)$$

Inserting $\nabla_{\mathbf{f}_i}R_{k,i}(\mathbf{f},\boldsymbol{\theta})$ and $\nabla_{\mathbf{f}_i}R_{k,\ell}(\mathbf{f},\boldsymbol{\theta})$ from (15) and (16), respectively, into (14) gives $\nabla_{\mathbf{f}_i}\tilde{\mathcal{R}}_{\mathrm{sum}}(\mathbf{f},\boldsymbol{\theta})$ expressed in (9), which completes the proof.

Appendix B
Proof of Theorem 2

From (6), it follows that

$$\begin{aligned}
&\nabla_{\boldsymbol{\theta}}\tilde{R}_{\mathrm{sum}}(\mathbf{f},\boldsymbol{\theta})\\
&=\sum_{g\in\mathcal{G}}\frac{\sum_{k\in\mathcal{K}_g}\Big[\exp\big\{-\tau R_{k,g}(\mathbf{f},\boldsymbol{\theta})\big\}\nabla_{\boldsymbol{\theta}}R_{k,g}(\mathbf{f},\boldsymbol{\theta})\Big]}{\sum_{k\in\mathcal{K}_g}\exp\{-\tau R_{k,g}(\mathbf{f},\boldsymbol{\theta})\}}. \qquad (17)
\end{aligned}$$

It is clear that we now need to find $\nabla_{\boldsymbol{\theta}}R_{k,g}(\mathbf{f},\boldsymbol{\theta})$, which is given by

$$\begin{aligned}
\nabla_{\boldsymbol{\theta}}R_{k,g}(\mathbf{f},\boldsymbol{\theta})&=\nabla_{\boldsymbol{\theta}}\ln\Big(1+\sum_{j\in\mathcal{G}}|\mathbf{z}_{k,g}\mathbf{f}_j|^2\Big)\\
&\quad-\nabla_{\boldsymbol{\theta}}\ln\Big(1+\sum_{\ell\in\mathcal{G}\setminus\{j\}}|\mathbf{z}_{k,g}\mathbf{f}_\ell|^2\Big)\\
&=\frac{\sum_{j\in\mathcal{G}}\nabla_{\boldsymbol{\theta}}|\mathbf{z}_{k,g}\mathbf{f}_j|^2}{1+\sum_{j\in\mathcal{G}}|\mathbf{z}_{k,g}\mathbf{f}_j|^2}-\frac{\sum_{\ell\in\mathcal{G}\setminus\{j\}}\nabla_{\boldsymbol{\theta}}|\mathbf{z}_{k,g}\mathbf{f}_\ell|^2}{1+\sum_{\ell\in\mathcal{G}\setminus\{j\}}|\mathbf{z}_{k,g}\mathbf{f}_\ell|^2}. \qquad (18)
\end{aligned}$$

Next, a closed-form expression for $\nabla_{\boldsymbol{\theta}}|\mathbf{z}_{k,g}\mathbf{f}_j|^2$ can be obtained as follows:

$$\begin{aligned}
&\nabla_{\boldsymbol{\theta}}|\mathbf{z}_{k,g}\mathbf{f}_j|^2=\nabla_{\boldsymbol{\theta}}\Big(\mathbf{z}_{k,g}\mathbf{f}_j\mathbf{f}_j^\dagger\big(\mathbf{z}_{k,g}\big)^\dagger\Big)\\
&=\nabla_{\boldsymbol{\theta}}\Big[\big(\mathbf{h}_{k,g}+\hat{\mathbf{h}}_{k,g}\boldsymbol{\Theta}\mathbf{H}_{\mathrm{ts}}\big)\mathbf{f}_j\mathbf{f}_j^\dagger\big\{(\mathbf{h}_{k,g})^\dagger+\mathbf{H}_{\mathrm{ts}}^\dagger\boldsymbol{\Theta}^\dagger\big(\hat{\mathbf{h}}_{k,g}\big)^\dagger\big\}\Big]\\
&\overset{(b)}{=}\mathrm{vec_d}\big\{\big(\hat{\mathbf{h}}_{k,g}\big)^\dagger\mathbf{z}_{k,g}\mathbf{f}_j\mathbf{f}_j^\dagger\mathbf{H}_{\mathrm{ts}}^\dagger\big\}, \qquad (19)
\end{aligned}$$

where (b) follows from [13, Table 4.3 and eqn. (6.153)]. Using (17)-(19), a closed-form expression for $\nabla_{\boldsymbol{\theta}}\tilde{\mathcal{R}}_{\mathrm{sum}}(\mathbf{f},\boldsymbol{\theta})$ is given by (10). This concludes the proof.

References

[1] D. Lecompte and F. Gabin, "Evolved multimedia broadcast/multicast service (eMBMS) in LTE-advanced: overview and Rel-11 enhancements," *IEEE Commun. Mag.*, vol. 50, no. 11, pp. 68–74, 2012.

[2] W. Guo, M. Fuentes, L. Christodoulou, and B. Mouhouche, "Roads to multimedia broadcast multicast services in 5G new radio," in *IEEE Int. Symp. Broadband Multimedia Syst. Broadcast. (BMSB)*, 2018, pp. 1–5.

[3] N. Sidiropoulos, T. Davidson, and Z.-Q. Luo, "Transmit beamforming for physical-layer multicasting," *IEEE Trans. Signal Process.*, vol. 54, no. 6, pp. 2239–2251, 2006.

[4] E. Karipidis, N. D. Sidiropoulos, and Z.-Q. Luo, "Quality of service and max-min fair transmit beamforming to multiple cochannel multicast groups," *IEEE Trans. Signal Process.*, vol. 56, no. 3, pp. 1268–1279, 2008.

[5] C. Pan *et al.*, "Reconfigurable intelligent surfaces for 6G systems: Principles, applications, and research directions," *IEEE Commun. Maga.*, vol. 59, no. 6, pp. 14–20, 2021.

[6] L. Du, W. Zhang, J. Ma, and Y. Tang, "Reconfigurable intelligent surfaces for energy efficiency in multicast transmissions," *IEEE Trans. Veh. Technol.*, vol. 70, no. 6, pp. 6266–6271, 2021.

[7] L. Du, S. Shao, G. Yang, J. Ma, Q. Liang, and Y. Tang, "Capacity characterization for reconfigurable intelligent surfaces assisted multiple-antenna multicast," *IEEE Trans. Wireless Commun.*, vol. 20, no. 10, pp. 6940–6953, 2021.

[8] Q. Tao, S. Zhang, C. Zhong, and R. Zhang, "Intelligent reflecting surface aided multicasting with random passive beamforming," *IEEE Wireless Commun. Lett.*, vol. 10, no. 1, pp. 92–96, 2021.

[9] G. Zhou, C. Pan, H. Ren, K. Wang, and A. Nallanathan, "Intelligent reflecting surface aided multigroup multicast MISO communication systems," *IEEE Trans. Signal Process.*, vol. 68, pp. 3236–3251, 2020.

[10] D. Li, Q. An, Y. Shi, and Y. Zhou, "Multigroup multicast transmission via intelligent reflecting surface," in *IEEE Veh. Technol. Conf. (VTC2020-Fall)*, 2020, pp. 1–6.

[11] F. Shu, G. Yang, and Y.-C. Liang, "Reconfigurable intelligent surface enhanced symbiotic radio over multicasting signals," in *IEEE Veh. Technol. Conf. (VTC2021-Spring)*, 2021, pp. 1–6.

[12] L. Dai *et al.*, "Reconfigurable intelligent surface-based wireless communications: Antenna design, prototyping, and experimental results," *IEEE Access*, vol. 8, pp. 45 913–45 923, 2020.

[13] A. Hjørungnes, *Complex-valued matrix derivatives: With applications in signal processing and communications*. Cambridge University Press, 2011.

[14] N. S. Perović, L.-N. Tran, M. Di Renzo, and M. F. Flanagan, "On the maximum achievable sum-rate of the RIS-aided MIMO broadcast channel," *arXiv preprint arXiv:2110.01700*, 2021.

[15] B. Feng *et al.*, "Optimization techniques in reconfigurable intelligent surface aided networks," *IEEE Wireless Commun.*, vol. 28, no. 6, pp. 87–93, 2021.

[16] Y. Nesterov, "Smooth minimization of non-smooth functions," *Math. Program., Ser. A*, vol. 103, pp. 127–152, 2005.

[17] L. Armijo, "Minimization of functions having lipschitz continuous first partial derivatives," *Pac. J. Math.*, vol. 16, no. 1, pp. 1–3, 1966.

[18] A. N. Iusem, "On the convergence properties of the projected gradient method for convex optimization," *Comp. App. Math.*, vol. 22, no. 1, pp. 37–52, 2003.